Calibration and Nonlinearity Compensation for Force Application in AFM based Nanomanipulation

Hui Xie, *Member, IEEE*, Julien Vitard, Sina Haliyo, and Stéphane Régnier

Abstract— Both the extent and accuracy of force application in atomic force microscope (AFM) nanomanipulation are significantly limited by the nonlinearity of the commonly used optical lever with a nonlinear position-sensitive detector (PSD). In order to compensate the nonlinearity of the optical lever, a nonlinear calibration method is presented. This method applies the nonlinear curve fit to a full-range position-voltage response of the photodiode, obtaining a continuous function of its voltage-related sensitivity. Thus, Interaction forces can be defined as integrals of this sensitivity function between any two responses of photodiode voltage outputs, instead of rough transformation with a single conversion factor. The lateral position-voltage response of the photodiode, a universally acknowledged puzzle, was directly characterized by an accurately calibrated force sensor composed of a tippless piezoresistive force sensor, regardless of any knowledge of the cantilevers and laser measuring system. Experiments using a rectangular cantilever (normal force constant 0.24 N/m) demonstrated that the proposed nonlinear calibration method restrained the sensitivity error of normal position-voltage responses to 3.6% and extended the force application range.

Index Terms — Atomic force microscope, nanomanipulation, force calibration, nonlinearity compensation.

I. INTRODUCTION

Atomic force microscope (AFM), brought into the world more than two decades ago [1], has been proved to be a significant and popular tool for various application of scientific and industrial interest. As an important application domain, AFM based nanomanipulation made a great progress in recent years. Various AFM based nanomanipulation systems and manipulation schemes have been developed [2-7]. In order to facilitate the nanomanipulation, haptic devices and virtual reality interfaces were introduced into the AFM based nanomanipulation systems [8, 9], thereby enabling an operator to directly interact with the real nano-world. Augmented reality systems brought us further development by updating the local virtual environment using real-time feedback of tip-nanoworld interaction [10, 11]. Employing the same interface, operators can further monitor real-time changes of the nano-environment through a movie-like AFM image [12]. Haptics and visualization provide us friendly interfaces to easily manipulate nano-objects.

However, highly precise position control of the AFM scanning stage and accurate detection of interaction forces between the AFM tip and nano-objects or nanoenvironment

are prerequisite to a successful nanomanipulation. Method and models were developed to compensate positioning errors in the AFM caused by drift, creep, hysteresis and other inherent nonlinearities [13, 14], aiming to overcome the spatial uncertainty and manipulate particles with sizes that are on the order of 10 nm. In most commercial AFM, the interaction forces between the AFM tip and nano-objects are detected by an optical lever, which mainly consists of a laser and a position-sensitive detector (PSD) [15]. Unfortunately, the limited linear range of the optical lever reduces the usable range and decreases the accuracy of the force application, especially when a soft cantilever is used. The calibration and nonlinearity compensation of the force application are therefore most necessary for the accurate nanomanipulation.

In order to calculate the absolute values of normal and lateral forces from AFM voltage signals, it is necessary to know the accurate value of the spring constant of the cantilever and the sensitivity of the optical lever. A number of methods have been developed for the spring constant calibration of the cantilever [16], one method most commonly adopted was developed by Cleveland *et al*. who utilized frequency shifts due to a known mass loaded on the free end of the cantilever [17]. The normal force applied to the tip can be simply calculated by multiplying the vertical deflection of the cantilever to its spring constant. In contrast, the lateral force calibration is more challenging to the normal calibration. Generally, two kinds of methods, two-step methods [18, 19] and direct methods [20–22] are commonly used. The two-step method involves the calibration of the torsional spring constant of the cantilever and the measurement of the lateral photodiode response. This method is not straightforward and is limited in application due to the measured lateral sensitivity of the photodiode should be significantly reduced due to the lateral contact stiffness between the tip and the sample [19, 20], which is often comparable to the lateral stiffness of the cantilever and its tip [23, 24].

The emphasis in this paper is the calibration and compensation for force application of the AFM based nanomanipulation system. For the lateral calibration, we present a new method to calibrate the lateral force measurement in the AFM using a commercially available, accurately calibrated piezoresistive force sensor, which consists of a piezoresistive cantilever and accompanying electronics, providing a force standard for the lateral force calibration of the AFM cantilever. During the force calibration, full range of the force-voltage data of normal and lateral application were recorded for the nonlinearity compensation of the optical lever. Compensation methods provide a means that allows

the accurate force application within the full detection range of optical lever. This paper is organized as follows: Section II simply describes the AFM based nanomanipulation system. In Section III, methods for the normal and lateral force calibration are proposed. Nonlinear compensation of the force application is discussed in the next section. Section V presents conclusion.

II. AFM BASED NANOMANIPULATION SYSTEM

The AFM based nanomanipulation system with an augmented virtual reality is equipped with a nanopositioning stage with a maximum range of 50 μm×50 μm on X-Y axes and 12 μm on Z axis. An optical microscope (Olympus BX50WI) is used to locate the laser spot on the cantilever and select the interested area for manipulation. The augmented reality consists of a PC based virtual environment and a haptic device (Virtuose 3D15-25, designed by CEA of France). These two subsystems are connected by the Ethernet. The eXtended Dynamical Engine (XDE) is employed to compute the occurring interactions in the mechanical model under the simulated environment. The augmented reality is designed in such a way that haptic control and vision computation run on different loops (30 Hz in visual loop and 1 kHz for the force feedback). Combining with the simulated, normal and lateral forces from the cantilever tip, the augmented reality provides us real forces feel and a real-time visual display in the simulated environment during the nanomanipulation.

III. CALIBRATION OF THE FORCE APPLICATION

A. Scheme for the force application

The key element in an AFM is a device for measuring the force applied on the tip. The commonly used optical lever, mainly composed of a laser and a PSD, is believed to be more sensitive and reliable detection device than others [15, 25]. As depicted in Fig. 1, this method makes uses of a photodiode consisting of two or four closely jointed segments to detect nanoscale deflection of the cantilever. Forces applied on the tip result in deflections of the cantilever, causing unbalanced signal output of the photodiode segments. These signals are further amplified by external electronics and then are employed as input signals for the forces feedback during the manipulation. For example, in our system, a quadrant photodiode is used to detect the normal and torsional signals by the electronics output $V_n = (V_{A1} + V_{A2}) - (V_{B1} + V_{B2})$ and $V_l = (V_{A1} + V_{B1}) - (V_{A2} + V_{B2})$, respectively. In order to convert these signals into forces, one need to calibrate the normal and lateral force factors β and α, by which the corresponding forces F_n and F_l are given by:

$$F_n = \beta \cdot V_n \tag{1}$$

$$F_l = \alpha \cdot V_l \tag{2}$$

where ΔV represents the change in the respective signal due to an applied force in the respective direction relative to any offset of the signal captured when no force is applied.
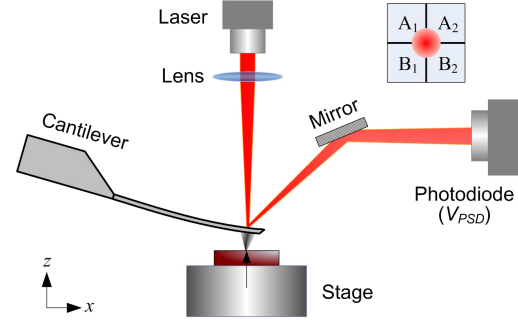

Fig. 1.   The optical lever in a typical atomic force microscope.

TABLE I

FORCE CALIBRATION RESULTS

$t(\mu m)$	k_n(N/m)	k_l(N/m)	$\beta(\mu N/V)$	$\alpha(\mu N/V)$
2.14	0.24	74.90	0.47 ± 0.02	14.85 ± 1.66

B. Normal force calibration

In experiments, a rectangular AFM cantilever with a normal force constant of 0.24 N/m was used. Although dimensions of the cantilever were provided by the manufacture, the cantilever's dimensions (L = 466 μm, l = 455 μm, w = 51.4 μm and h = 16.5 μm) were measured under the optical microscope, where L, l, w and h are the length, effective length, width, thickness and tip height of the cantilever, respectively. Forced oscillation was employ to determine the thickness t of the cantilever. If we know the resonant frequencies of the cantilever, t can be obtained by [26]:

$$t = \frac{\omega_n}{K_n^2} \cdot \sqrt{\frac{12\rho}{E}} \tag{3}$$

where K_n is the wave number on the cantilever, ω_n is the nth flexural resonant frequency. If $n = 1$, then $K_n L = 1.8751$. Its normal and lateral spring constants k_n and k_l can be calculated by:

$$k_n = \frac{Ewt^3}{4L^3} \quad k_l = \frac{Gwt^3}{3L(h + t/2)} \tag{4}$$

When the normal spring constant k_n is known, the normal force can be calculated by:

$$\beta = \frac{k_n \delta_n}{\Delta V_n} \tag{5}$$

where δ_n is the bending deflection on the tip of the cantilever, ΔV_n is the corresponding voltage output of the photodiode. The next step is to calibrate the normal force factor β. In our experiment, the cantilever's tip contacted with a glass loading button. A Z nanostage (resolution 1.8 nm) was employed for the precisely loading on the cantilever tip. After slightly touching the button, the Z nanostage was moved upward with an increment of 5 nm in the frequency of 1 Hz. After 20 complete calibration cycles, the normal force factor β of this cantilever was calibrated as 0.47 μN/V using a linear fit 40% of the total range of the photodiode response (see Fig. 4(a)). The calibration results are shown in Table I.
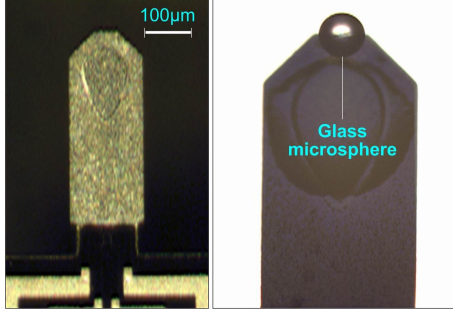
Fig. 2. Top image of the piezoresistive cantilever (left). (Right) a glass microsphere attached on the tip of the piezoresistive cantilever.
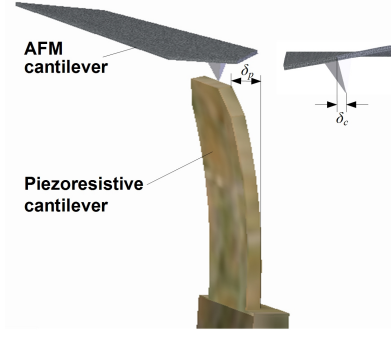

Fig. 3. Scheme of the experimental configurations for the calibration of the AFM with a piezoresistive force sensor. The deflection of the piezoresistive and testing cantilever are δ_p and δ_c respectively.

C. Lateral force calibration

1) Calibration of the piezoresistive force sensor: A piezoresistive cantilever (Nascatec GmbH, Germany) and its electronics are commercially available in our work. Microscopy images of the piezoresistive are shown in Fig. 2. Dimensions of the piezoresistive cantilever were measured as 525.8 μm in length and an average width of 152.7 μm. The piezoresistive cantilever stiffness k_p was calibrated using mass loading method [17]. Six glass micro spheres with diameters from 25.6 μm to 64.4 μm were placed in sequence on the free end of the piezoresistive cantilever and their centers were also measured by the optical microscope for stiffness compensation due to position errors. The stiffness of the piezoresistive cantilever was calibrated at $k_p = 18.209 \pm 0.471$ N/m. In the force sensitivity calibration, the Z nanostage (resolution 1.8 nm) with an attached glass substrate was used for the displacement increments during the calibration. A program was used to control the nanostage motion with a fixed increment of 20 nm while the voltage output V_p of the electronics was recorded. After 20 complete loading/unloading calibration cycles, A piezoresistive force sensitivity $S_p = 10.361 \pm 0.267$ μN/V was achieved.

2) Lateral calibration of the AFM cantilever: After calibration, the piezoresistive force sensor was used as a force standard to determine the conversion factors α of the AFM cantilevers. The piezoresistive cantilever was mounted vertically on the AFM stage along its longitudinal axis (see Fig. 3). In this case, the tip of the testing cantilever contacts the top end of the piezoresistive cantilever in the lateral calibration. After the AFM cantilever was brought into contact with the top surface of the piezoresistive cantilever, the contact mode was used to scan the top side edge to identify its center point. Then the AFM cantilever was moved 2 μm away from the scanned side edge. In order to ensure the AFM tip was in contact with the top side edge, the AFM cantilever was moved down with a displacement $\Delta h = 0.5 - 0.8$ μm before being moved back to the loading location which is on the top edge of the piezoresistive force sensor, thus, the lateral force conversion factor α can be simplified obtained by:

$$\alpha = \frac{F_t}{V_l} = \frac{S_p V_p}{V_l} \tag{6}$$

where V_p and V_l are voltage outputs of the piezoresistive force sensor and the photodiode, respectively. Each cantilever was laterally bent by the piezoresistive cantilever for ten times. The factor α was averaged from ten times of experimental results (a full range lateral response is shown in Fig. 4(b)). The experimental results are summarized in Table I.

IV. COMPENSATION OF THE FORCE CALIBRATION

A. Traditional Force calibration

Various literatures analyzed and discussed the characterization of the optical lever sensitivity [27-29]. The sensitivity of the optical lever can be enhanced by increasing the intensity of the laser beam or by decreasing the beam divergence. Moreover, during the force calibration, the sensitivity of the optical lever has strong dependences on the position of the laser spot relative to the center of the PSD and geometry of the optical path [19, 30]. Main causes that introduce the nonlinearities are the shape and intensity distribution of the laser spot on the PSD [31], which limit the range of real force application in AFM. For the traditional force calibration of the AFM, the photodiode sensitivity S_{PSD} is considered as linear response to the force applied on cantilever's tip by:

$$S_{PSD} = \frac{V_{PSD} - V_{PSD}^0}{\delta_p} \tag{7}$$

where and are the voltage output of the photodiode before and after the force loading, δ_p is the tip deflection with a force loading. Actually, the photodiode sensitivity S_{PSD} is not constant, that is the plot of the photodiode voltage output V_{PSD} versus the applied force is nonlinear. In fact, our experiments indicated that more than 200 variation in S_{PSD} is a function of the range and initial value of the photodiode voltage output. The force-voltage response of the AFM therefore should be accurately calibrated in the full range of the photodiode.

B. Nonlinear compensation of the force application

For the convenience of normal and lateral calibration, angular sensitivity S_{PSD} was used in our experiments. The normal photodiode sensitivity is defined as S_{PSD}^n and the lateral sensitivity S_{PSD}^l. θ_n and θ_l are the normal and lateral

angular deflections of the cantilever. The normal spring constant k_n connects the flexural deflection δ_n due to an applied normal force $F_n = k_n \delta n$. So based on the beam mechanics, θn can be presented as:

$$\theta_n = \frac{3}{2l} \cdot \frac{F_n}{k_n} \tag{8}$$

where l is the effective length of the cantilever. Thus, if we know the continuous function of V_{PSD}^n, S_{PSD}^l can be determined by:

$$S_{PSD}^n = \frac{2l}{3} \cdot \frac{dV_{PSD}^n}{d\delta_n} \tag{9}$$

For a rectangular cantilever, the torsional angle θ_l related to the applied force F_l by:

$$\theta_l = \frac{3F_l l(h + t/2)}{Gwt^3} \tag{10}$$

where G is the shear modulus. Thus the lateral sensitivity of the photodiode can be also determined by:

$$S_{PSD}^l = \frac{dV_{PSD}^l}{d\theta_l} \tag{11}$$

Continuous functions of the normal and lateral sensitivities can be determined by the calibration and nonlinear fit of the position-voltage curves. Thus, in the actual application, the angular deflection of the cantilever can be obtained by:

$$\theta_n = \int_{V_{PSD}^{n0}}^{V_{PSD}^{n1}} S_{PSD}^{n}{}^{-1} dV_{PSD}^n \tag{12}$$

$$\theta_l = \int_{V_{PSD}^{l0}}^{V_{PSD}^{l1}} S_{PSD}^{l}{}^{-1} dV_{PSD}^l \tag{13}$$

where the lower and upper limits are the initial and force deduced voltage outputs of the photodiode. Also the normal and lateral tip displacement can be calculated by:

$$\delta_n = \frac{2l}{3}\theta_n \tag{14}$$

$$\delta_l = \theta_l(h + t/2) \tag{15}$$

In the actual application, the whole nonlinear calibration protocol can be carried as follows:

- Set the initial voltage output (without force loading) of the photodiode near the lower point by adjusting the position of reflecting laser spot.
- Record original force/position-voltage responses by the normal and lateral force calibration.
- Transform the force/position-voltage responses to voltage-angular sensitivity responses by (8) and (10) for normal and lateral cases, respectively.
- Employ the nonlinear fit of the voltage-angular sensitivity response to obtain a continuous function of voltage output V_{PSD} and then calculate the angular sensitivity S_{PSD} by (9) and (11).
- Calculate the angular deflection on the AFM tip using (12) and (13) for normal and lateral force application, respectively. Then the applied forces on the AFM tip can be easily obtained.

C. Experimental results

The experiments described below were performed on an AFM based nanorobotic system. The voltage range of the position detector, unlike ± 10 V of a commercial AFM, is ± 1.5 V because electronics is with a lower ratio of signal amplifier. Nonetheless, the general approach can be widely applicable and the only difference is just the calibrated conversion parameters described in Table I. Inspired by the sigmoidal shape of the V_{PSD} versus θ plots presented in Fig. 4, the method of Sigmoidal fit was employed to the normal and lateral voltage-angular sensitivity response (V_{PSD}, θ) in the experiments. The common Dose response function was used in the Sigmoidal fit by:

$$V_{PSD} = A_1 + \frac{A_2 - A_1}{1 + 10^{(\theta^0 - \theta)p}} \tag{16}$$

where A_1, A_2, p and θ_0 are the nonlinear fit parameters: lower limit, upper limit, slope and the value of θ as half value of V_{PSD}. All the responses are in the almost full range of the photodiode signal output. The next step is to calculate the inverse angular sensitivities of the photodiode, which can be obtained as the derivative of the Sigmoidal fit in (16):

$$S_{PSD}^{-1} = \frac{d\theta}{dV_{PSD}} = \frac{(1 + \xi)^2}{(A_2 - A_1)\xi p \ln 10} \tag{17}$$

where $\xi = (A_2 - V_{PSD})/(A_1 - V_{PSD})$. Thus, we get a continuous function of the angular sensitivity S_{PSD} on the full range of photodiode voltage output V_{PSD}, rather than a single value. This function will be used to calculate the compensated normal and lateral angular deflections by (12) and (13) (rather than from (8) and (10), which assumes a linear transform between applied force and deflection with a single value of the sensitivity S_{PSD}), respectively. So a simple expression of the angular deflection between any two signal outputs and can be obtained by:

$$\theta = -\frac{\ln|\xi|}{2.302585 \cdot p} \Big|_{V_{PSD}^0}^{V_{PSD}^1} \tag{18}$$

Voltage-angular deflection responses (V_{PSD}, θ) of the normal and lateral cases used for the calculation of the photodiode sensitivities S_{PSD} were obtained by the real force calibrations with a soft cantilever that has a normal spring constant of 0.24 N/m. The Dose response function was used to fit the (V_{PSD}, θ)) responses and fitting parameters are shown in Table II, which would be used to calibrate the sensitivity S_{PSD} via (18). Sigmoidal fit results are shown in Fig. 4, including the force calibration curves (V_{PSD}, θ) (open circle) and fitting results using the Dose response function (red line). Fig. 4 (a) shows the normal V_{PSD}) versus θ_n response, and the lateral V_{PSD} versus θ_n response is presented in Fig. 4(b). All the responses are in the almost 95% full range of the photodiode output (± 1.43V). For the lateral force calibration, the angular deflection is calculated via (10) with the readout of the piezoresistive force sensor.

In order to further verify the proposed method for the nonlinearity compensation, an apparent sensitivity compensation experiment was evaluated using the response of the
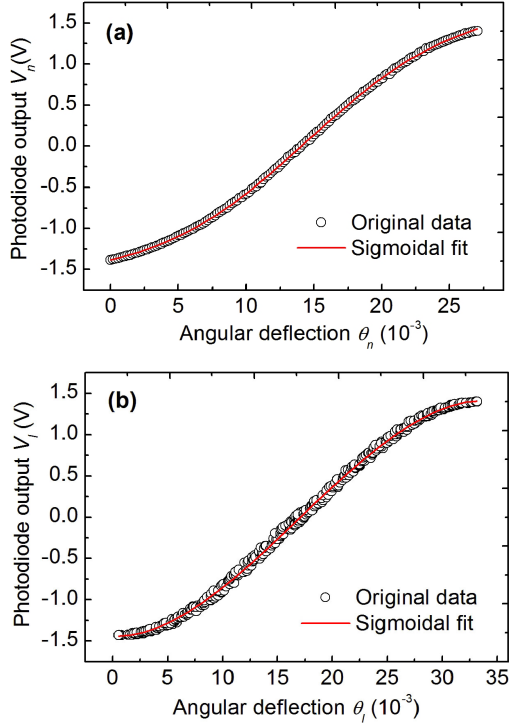
Fig. 4. The force calibration curves (V_{PSD}, θ) and Sigmoidal fitting results using the Dose response function. (a) V_{PSD}^{n} versus θ_{n} response. (b) V_{PSD}^{l} versus θ_{l} response.

TABLE II
PARAMETERS OF THE SIGMOIDAL FIT

Calibration Type	A_1	A_2	θ_0	p
Normal	-1.62358	1.76318	14.55008	0.07663
Lateral	-1.61967	1.71585	16.98019	0.06446

normal inverse S_{PSD} versus the normal voltage V_n. Fig. 5(a) shows that more than 200% variation in normal S_{PSD} is the function in the full range of the photodiode voltage output. The fitting sensitivity (red line) generated from the Sigmoidal fit is in accordance with the shape of the real sensitivity curve. The blue straight line, obtained from a linear fit of the bottom on the real sensitivity curve, indicates that an inverse sensitivity 6.92×10^{-3} rad/V is the minimum value of this curve, presenting the highest sensitivity when the laser spot is near the center of the photodiode. For easier representation the results of the sensitivity compensation, the ratio of the real and the fitting sensitivity was multiplied by the minimum inverse sensitivity in Fig. 5(a), giving an apparent compensated sensitivity as shown in Fig. 5(b). The slope of the linear fit of the compensated sensitivity is 0.087 (red line), resulting in a variation of 3.6% in contrast with more than 200% before the compensation. The range of the force measurement was extended from 36% to 95% of the represents 36% of the full range of ± 1.5 V, and the corresponding force application range improved from 0.25
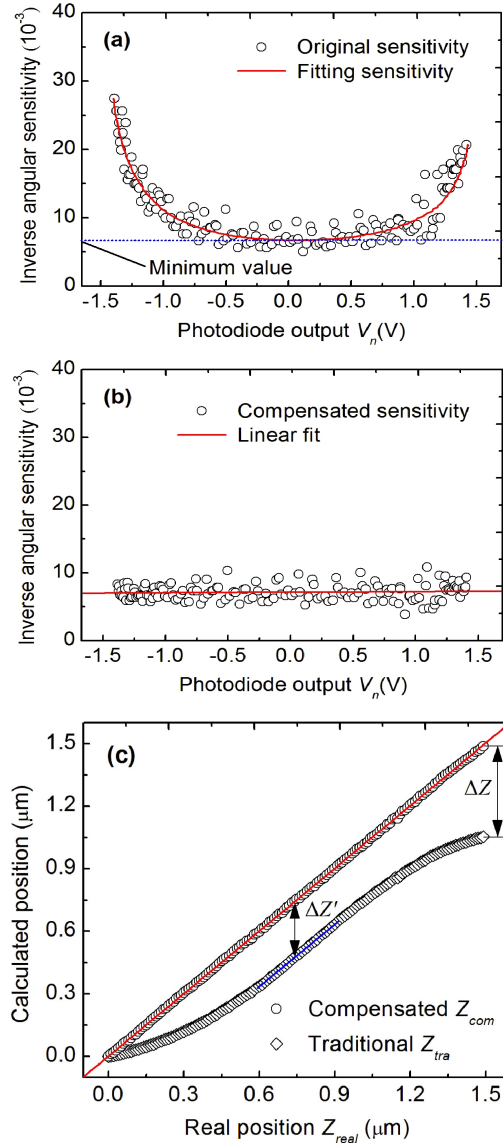

Fig. 5. (a) The normal inverse sensitivity versus normal voltage as the slope $d\theta/dV_{PSD}$ of the normal (V_{PSD}, θ_n) response shown in Fig. 4(a). (b) Compensated normal inverse sensitivity using Sigmoidal fit of data shown in Fig. 5(a). (c) Compensated position Z_{com} and traditional calibrated Z_{tra} versus real position Z_{real} recorded by the AFM stage.

μN to 0.69 μN of the cantilever with a spring constant of 0.24 N/m. Fig. 5(c) shows the further comparison of the positions calculated from the traditional and the proposed method. The diamond symbol shows a nonlinear relationship between the calculated positions by traditional method Z_{tra} versus real position Z_{real} recorded by the AFM stage, resulting in an overall position error $\Delta z = 0.434$ μm (28.9% of the total displacement in the full range of the photodiode). The symbol of the circles displays an approximately straight line of compensated position Z_{com} with a gradient of 0.9996. Note that both plots have a same value of the linear fit near

the center of the photodiode, where the position difference keeps constant due to the linear sensitivity in this area. The experiments results indicated that an excellent nonlinear fit obtained by the proposed method.

V. Conclusion

In order to obtain highly-precise force detection and extend the force application range of the AFM based nanomanipulation system, the normal and lateral force applications were accurately calibrated and the corresponding nonlinear sensitivities were well compensated by the proposed method. For the calibration of the lateral force, a new method, making use of an accurately calibrated piezo-force sensor composed of a tippless piezoresistive cantilever and corresponding electronics, was employed to determine the lateral force conversion factor. This method may be used to directly calibrate factor between the lateral force and the photodiode signal for cantilevers with a wide range of spring constant, regardless of their size, shape, material or coating effect and any knowledge of the optical lever. A practicable approach was developed to compensate the sensitive nonlinearity of photodiode by calculating the cantilever deflection using the nonlinear fit of the sensitivity, which was achieved from the Sigmoidal fit of the normal and lateral force-voltage curves, thereby extending the effective force application range of the optical lever. The experimental results demonstrated that the sensitivity error of normal responses could be reduced from more than 200% to 3.6% and the range of the accurate force application was extended.

VI. Acknowledgments

References

[1] G. Binning, C. F. Quate, and C. Gerber, "Atomic force microscope," *Phys. Rev. Lett.*, vol. 56, no. 9, pp. 930-933, 1986.

[2] J. A. Stroscio, and D. M. Eigler, "Atomic and molecular manipulation with the scanning tunneling microscope," *Science*, vol. 254, no. 5036, pp. 1319-1326, 1991.

[3] T. Junno, K. Deppert, L. Montelius, and L. Samuelson, "Controlled manipulation of nanoparticles with an atomic force microscope," *Appl. Phys. Lett.*, vol. 66, no. 26, pp. 3627-3629, 1995.

[4] C. Baur, A. Bugacov, B. E. Koel, A. Madhukar, N. Montoya, T. R. Ramachandran, A. A. G. Requicha, R. Resch, and P. Will "Nanoparticle manipulation by mechanical pushing: underlying phenomena and real-time monitoring," *Nanotechnology*, vol. 9, no. 4, pp. 360-364, 1998.

[5] R. Resch, D. Lewis, S. Meltzer, N. Montoya, B. E. Koel, A. Madhukar, A.A.G. Requicha, and P. Will, "Manipulation of gold nanoparticles in liquid environments using scanning force microscopy,"*Ultramicroscopy*, vol. 82, no. 1, pp. 135-139, 2000.

[6] P. Dieska, and I. Stich, "Nanomanipulation Using Only Mechanical Energy," *Phys. rev. lett.*, vol. 95, no. 12, pp. 126103, 2005.

[7] J. Hu, Y. Zhang, B. Li, H. B. Gao, U. Hartmann, and M. Q. Li, "Nanomanipulation of single DNA molecules and its applications," *Surf. Interf. Anal.*, vol, 36, no. 2, pp. 124-126, 2004.

[8] S. G. Kim, and M. Sitti, "Task-based and stable tele-nanomanipulation in a nanoscale virtual environment," *IEEE Trans. Autom. Sci. Eng.*, vol. 3, no. 3, pp. 240-247, 2006.

[9] M. Sitti, and H. Hashimoto, "Teleoperated touch feedback of surfaces at the nanoscale: Modeling and experiments," IEEE/ASME Trans. Mechatronics, vol. 8, no. 2, pp. 287-298, 2003.

[10] G. Y. Li, N. Xi, M. M. Yu, and W. K. Fung, "Development of augmented reality system for AFM-based nanomanipulation," *IEEE/ASME Trans. Mechatronics*, vol. 9, no. 2, pp. 358-365, 2004.

[11] W. Vogl, B. Kai. L. Ma, and M. Sitti, "Augmented Reality User Interface for an Atomic Force Microscope based Nanorobotic System," *IEEE Trans. Nanotechnology*, vol. 5, no. 4, pp. 397-406, 2006.

[12] G. Y. Li, N. Xi, H. P. Chen, C. Pomeroy, and M. Prokos, "Videolized' atomic force microscopy for interactive nanomanipulation and nanoassembly," *IEEE Trans. Nanotechnology*, vol. 4, no. 5, pp. 605-615, 2005.

[13] B. Mokaberi, and A. A. G. Requicha, "Drift compensation for automatic nanomanipulation with scanning probe microscopes," *IEEE Trans. Autom. Sci. Eng.*, vol. 3, no. 3, pp. 199-207, 2006.

[14] B. Mokaberi, and A.A. G. Requicha, "Compensation of scanner creep and hysteresis for AFM nanomanipulation," *IEEE Trans. Autom. Sci. Eng.*, Accepted for future publication.

[15] G. Meyer, and N. M. Amer, "Novel optical approach to atomic force microscopy,"*Appl. Phys. Lett.*, vol. 53, no. 12, pp. 1045-1047, 1988.

[16] N. A. Burnham, X. Chen, C. S. Hodges, G. A. Matei, E. J. Thoreson,C. J. Roberts, M. C. Davies, and S. J. B. Tendler, "Comparison of calibration methods for atomic-force microscopy cantilevers," *Nanotechnology*, vol. 14, no. 1, pp. 1-6, 2003.

[17] J. P. Cleveland, S. Manne, D. Bocek, and P. K. Hansma, "A Nondestructive method for determining the spring constant of cantilevers for Scanning force microscope," *Rev. Sci. Instrum.*, vol. 64, no. 2, pp. 403-405, 1993.

[18] R. G. Cain, S. Biggs, and N. W. Page, "Force Calibration in Lateral Force Microscopy," *J. colloid interf. Sci.*, vol. 227, no.1, pp. 55-65, 2000.

[19] R. J. Cannara, M. Eglin, and R. W. Carpick, "Lateral force calibration in atomic force microscopy: A new lateral force calibration method and general guidelines for optimization," *Rev. Sci. Instrum.*, vol. 77, no. 5, pp. 053701, 2006.

[20] D. F. Ogletree, R. W. Carpick, and M. Salmeron, "Calibration of frictional forces in atomic force microscopy," *Rev. Sci. Instrum.*, vol. 67, no. 9, pp. 3298-3306, 1996.

[21] M. Varenberg, I. Etsion, and G. Halperin, "An improved wedge calibration method for lateral force in atomic force microscopy," *Rev. Sci. Instrum.*, vol. 74, no. 7, pp. 3362-3367, 2003.

[22] H. Xie, J. Vitard, S. Haliyo, S. Régnier, and M. Boukallel, "Calibration of lateral force measurements in atomic force microscopy with a piezoresistive force sensor," *Rev. Sci. Instrum.*, vol. 79, no. 3, pp. 033708, 2008.

[23] R. W. Carpick, D. F. Ogletree, and M. Salmeron, "Lateral stiffness: A new nanomechanical measurement for the determination of shear strengths with friction force microscopy," *Appl. Phys. Lett.*, vol. 70, no.12, pp. 1548-1550, 1997.

[24] M. A. Lantz, S. J. O'shea, A. C. F. Hoole, and M. E. Welland, "Lateral stiffness of the tip and tip-sample contact in frictional force microscopy," *Appl. Phys. Lett.*, vol. 70, no. 8, pp. 970-972, 1997.

[25] S. Alexander, L. Hellemans, O. Marti, J. Schneir, V. Elings, and P. K. Hansma, "An atomic-resolution atomic-force microscope implemented using an optical lever," *J. Appl. Phys.*, vol. 65, no.1, pp. 164-167, 1989.

[26] D. A. Mendels, M. Lowe, A. Cuenat, M. G. Cain, E. Vallejo, D. Ellis, and F. Mendels, "Dynamic properties of AFM cantilevers and the calibration of their spring constants," *J. Micromech. Microeng.*, vol. 16, no. 8, pp. 1720-1733, 2006.

[27] D. Sarid, *Scanning Force Microscopy*, Oxford University Press, Oxford, 1991.

[28] J. Colchero, H. Bielefeldt, A. Ruf, M. Hipp, O. Marti, and J. Mlynek, "Scanning Force and Friction Microscopy," *Phys. Stat. Sol. (a)*, vol. 131, no. 1, pp. 73-75, 1992.

[29] T. E. Schaffer, and P. R. Hansma, "Characterization and optimization of the detection sensitivity of an atomic force microscope for small cantilevers" *J. Appl. Phys.* vol. 84, no.9, pp. 4661-4666, 1998.

[30] L. Y. Beaulieu, M. Godin, O. Laroche, V. Tabard-Cossa, and P. Grtter, "Calibrating laser beam deflection systems for use in atomic force microscopes and cantilever sensors," *Appl. Phys. Lett.*, vol, 88, no. 8, pp. 083108, 2006.

[31] T. E. Schaffer, and P. R. Hansma, "Characterization and optimization of the detection sensitivity of an atomic force microscope for small cantilevers," *J. Appl. Phys.*, vol. 84, no. 9, pp. 4661-4666, 1998.